On the Current and Future Capability of Parameter Estimation Methods of Compact Binary Coalescence events through measured Gravitational Waves via LIGO, VIRGO, and Cosmic Explorer

Sterling Scarlett*
Boston University Commonwealth Ave, Boston, MA 02215
LIGO Summer Undergraduate Research Fellowship program

Mentors: Alan Weinstein† and Jacob Golomb‡
Division of Physics, California Institute of Technology,
1200 E. California Blvd, Pasadena, CA 91125, USA
(Dated: September 22, 2024)

We introduce, understand, and interpret parameter estimation (PE), examining its role in analyzing Compact Binary Coalescence events (CBC) via their emission of Gravitational Waves (GW) and the measured GW strains by instruments such as LIGO, VIRGO, and the future detector Cosmic Explorer (CE). We explain and list all fifteen parameters that characterize of CBC. Understanding and looking at current methods of parameter estimation *(Bayesian inference likelihood based, Likelihood-free Simulation based, Fisher Matrix)*, we investigate how each method is currently used *(Bilby)*, future possibilities of the methods via machine learning *(Dingo)*, and advancements in detectors *(Cosmic Explorer)*. Conducting a comparative quantitative analysis with a methodology considering the speed, accuracy, and precision of the different methods and detectors, we aim to assess their efficiency and capabilities, offering insight on the future of PE of CBC events. We evaluate simulated events developed from a ***IMRPhenomXPHM*** waveform approximation and similar phenomenological frequency-domain waveform approximations to develop our injections of a full spectrum of CBC events. Doing this allows us to measure greater accuracy, precision, and characterization of potential strengths and weaknesses of each PE model and detector.

Keywords: Parameter Estimation, Compact Binary Coalescence, Bayesian Inference, Fisher Matrix, Bilby, Dingo, Cosmic Explorer

I. INTRODUCTION

Gravitational Waves (GW), predicted by General Relativity and detected by instruments like The Laser Interferometer Gravitational-Wave Observatory (LIGO), offer a window into the universe and provide data for understanding natural phenomena such as compact binary coalescence (CBC). Compact binaries are systems consisting of two compact astronomical objects. Members of this class include binary black holes (BBH), binary neutron stars (BNS), or one of each (NSBH). Coalescence describes all three stages of the collision of compact binaries. First, the objects' decaying orbits draw each other closer until they fully "Inspiral", in which the pair is losing energy and spiraling towards each other. Then they merge into one, and lastly, the object stabilizes, forming one body; this stage is called "Ringdown". We therefore define CBC as a system of two compact objects inspiring, merging and stabilizing into ringdown (IMR), producing GW in each stage.

When LIGO detects GWs, we analyze the data compared to waveform templates and then preform Parameter Estimations (PE), constructing developing distributions of were the the parameters of the event may exist at. There exist multiple methods to preform PE but Bayesian inference methods such Bilby stand as the industry standard and are the most accurate and precise. Following this, the simulation based likelihood-free method Dingo, represents a new frontier of PE not yet fully explored nor understood. Lastly, a Fisher matrix approach to PE such as GWfish represents merely a fast, rough approximation. While this is the current state of PE methods, science is always evolving and changing. Understanding this prompts our interest in the comparison of these methods in this paper, with goals of providing quantitative and qualitative understanding of how the current state of PE is, and provide future predictions on possible changes that it may hold.

This paper is structured as follows: Section II gives a brief introduction to different type of compact mergers, section **A** lists and defines all the astronomical parameters of CBC, highlighting both the intrinsic and extrinsic parameters. Section **B** offers an explanation of the population of CBC events and of exceptional events that exist in the distribution. Section **C** offers a discussion on the current PE methods, addressing briefly how both Bayesian inference, Simulation based, and Fisher matrix methods work, highlighting the current codes that use them and where their strengths and weaknesses lie. Sec-

* sterling.scarlett3@gmail.com
† ajw@caltech.edu
‡ jgolomb@caltech.edu

tion **III** of this paper defines the objectives of the research, indicating what we hope to accomplish and how we will do it. Section **IV** defines the approach and overall methodology we take in our comparative analysis study of PE methods, understanding the process behind our study and defining the steps we take in data simulation, PE, analysis, and explaining anything abstained in our study. Section **V** discusses our data analysis and initial interpretations; Section VI gives our conclusions and final interpretations of the data. Section VII discusses the future of our work as a whole. In Section VIII, we give our thanks and acknowledgements. Lastly, Appendix A shows examples tables of numerical data, and supporting information.

II. CBC AND PARAMETER ESTIMATION

As state previously GW carry details about the merging systems, usually BBH, allowing for parameter estimations of the source and resulting object [1]. Though compact binaries are the focus of this research, compact mergers are not limited to binaries. There exist different classes of mergers, an example are mergers from hierarchical triple-star systems or triples. These are systems organized as an inner, binary pair with a more distant, outer (tertiary) component [2–4].

Parameter	Symbol
Primary mass ($M_\odot$)	m_1
Secondary mass ($M_\odot$)	m_2
Time of coalescence (s)	t_c
Spin magnitudes	χ_1, χ_2
Sky position (RA,DEC) (rad)	α,δ
Reference phase (rad)	ϕ_c
Luminosity distance (Mpc)	d_L
Inclination angle (rad)	θ_{JN}
Spin angles (rad)	$\theta_1, \theta_2, \phi_{12}, \phi_{JL}$
Polarization angle (rad)	ψ

TABLE I. Astrophysical parameters of CBC events with corresponding units.

A. Astronomical parameters of *CBCs*

Focusing on CBC, as shown in TABLE I, the gravitational waveform formed by these events is characterized by fifteen parameters, eight "intrinsic" $(m_1, m_2, \chi_1, \chi_2, \theta_1, \theta_2, \phi_{12}, \phi_{JL})$, each angle being measured in radians, and seven "extrinsic" $(t_c, \alpha, \delta, \phi_c, d_L, \theta_{JL}, \psi)$:

- **Source-frame component masses** (m_1, m_2) - the mass of the larger object involved in the merger (**primary mass** m_1) and mass of the smaller object (**secondary mass** m_2), both are measured in Solar masses $M_\odot$. Given the speed and distance of these mass, the masses are red shifted, and by the time they reach they reach the detector frame they are m/c;
- **Time of coalescence** (t_c) - the time when the binary system merges, as measured at the geocenter (center of the Earth). This measurement is taken in GPS time, which is the time in seconds since January 6, 1980.
- **Sky position** (α, δ) - the location of the event on the celestial sphere in right ascension α and declination δ measured in radians.
- **Reference phase** (ϕ_c) - a reference point in the waveform used to describe the phase of the gravitational wave signal at the time of coalescence;
- **Luminosity distance** (d_L) - In cosmology there are many distance measurements such as Redshift z, the stretching of the wavelength of light as it travels through space, and Comoving distance D_{CM}, distance obtained by integrating the proper distances of nearby fundamental observers along the line of sight. Luminosity distance though is defined as the distance from the observer to the binary system, calculated based on the observed amplitude of the gravitational wave signal and its intrinsic strength measure in Mpc.
- **Inclination angle** (θ_{JN}) - the angle between the total angular momentum vector of the binary system and the line of sight from the observer to the source;
- **Polarization angle** (ψ) - the angle that describes the orientation of the polarization of the gravitational wave signal relative to the line of sight from the observer to the source.
- **Spin magnitudes** (χ_1, χ_2) - The spins of each binary object can specified by a 3-vector quantity denoting each component of the spin (χ_x, χ_y, χ_z), (χ_1, χ_2) are the magnitude of this 3 vector quantity aligned with the angular momentum starting at some reference frequency, usually 20 Hz.
- **Spin angles** ($\theta_1, \theta_2, \phi_{12}, \phi_{JL}$) - the various angles that are referenced to the orbital angular momentum $\hat{L}$ and the total angular momentum $\vec{J} = \vec{L}+\vec{S_1}+\vec{S_2}$. The individual spin angles θ_1, θ_2 change very little throughout CBC but given that the 3-vector quantity denoting spins are precessing , this causes both ϕ_{12}, ϕ_{JL} to change through the event.

While these fifteen parameters describe CBC, they are not the only quantities that can be measured from GW strain data. Other parameters, derived from the 15 can be defined, such as:

- **Effective Inspiral spin magnitude** (χ_{eff}) - given by

$$\chi_{\text{eff}} = \frac{(M_1\chi_1 \cos\theta_1 + M_2\chi_2 \cos\theta_2)}{M_1 + M_2},$$

the effective inspiral spin magnitude describes the influence of the individual spins of the two objects in a binary system on the gravitational wave signal during the inspiral phase. It accounts for the projection of the spins along the orbital angular momentum and is particularly important in determining how the spins affect the binary's orbital dynamics.χ_{eff} is particularly important because it remains approximately constant during the inspiral phase, even though the individual spins may precess. It provides a measure of how aligned or anti-aligned the spins are with the orbital angular momentum, influencing the waveform's evolution and the final spin of the merged object. A positive χ_{eff} indicates that the spins are preferentially aligned with the orbital angular momentum, while a negative value suggests anti-alignment. Although the individual spins are difficult to constrain, χ_{eff} is one of the most accurate measured parameters in CBC events.

- **Signal-to-noise ratio** (snr) - measurements of the strength of the gravitational wave signal compared to the background noise in the detectors;

- **Radiated energy** (E_{rad}) - The energy radiated in (GW) during the merger, typically measured in $ergs$. This energy corresponds to the difference between the total initial mass of the binary system and the final mass after the merger. The equation representing the energy lost in the form of gravitational waves is given by:

$$E \approx (M_{tot} - M_f)c^2$$

- **Peak Luminosity** (L_{peak}) – This refers to the maximum brightness or energy output per second emitted during an astrophysical event, typically derived from advanced numerical relativity simulations. It is commonly measured in units of $erg\,s^{-1}$.

- **Orbital precession** (δ, ϕ) - In Newtonian systems, precession is defined as the combination of Apsidal precession, where the major axis of an elliptical orbit cycles its orientation within its orbital plane, and Nodal precession, where non-spherical objects cause orbiting objects to change their orbits. Given that CBC are post-Newtonian systems, the precession of their system is not caused by this but rather is caused by explicit spin-orbit interaction term found in the Lagrangian.

- **Mass Ratio** (q) - As with luminosity distance, there are different types of mass ratios, such as the total mass, the mass ratio comparing the individual masses to the final mass, and the symmetric mass ratio, which is defined as $\eta = \frac{m_1 m_2}{(m_1+m_2)^2}$. The mass ratio q is defined as $q = \frac{m_2}{m_1}$, where $q < 1$.

- **Chirp mass**($\mathcal{M}$) - The chirp mass given by the equation

$$\mathcal{M}_c = M_{tot} * \eta^{\frac{3}{5}},$$

in which M_{tot} is the total mass of the system

$$M_{tot} = m_1 + m_2.$$

The chirp mass being this specific combination of the two individual masses in the binary system, plays a dominant role in determining the rate at which the two objects spiral toward each other due to the emission of gravitational waves. It is crucial parameter in the analysis of compact binary coalescence (CBC) signals as it governs the evolution of the gravitational wave frequency over time. The greater the chirp mass, the faster the inspiral, and the more detectable the signal becomes. It is often one of the most easily measurable parameter in a gravitational wave event and provides critical insights into the nature of the merging objects.

- **Final Mass** (M_f) - the Final mass is the mass of the resulting black hole after the merger. Given that energy is radiated in the merger, the Final Mass will be less than the combination of the component masses, refereed to as Total Mass.

- **Final Spin** (χ_{final}) - The final spin of the merged object resulting from a compact binary coalescence (CBC) event, describing the dimensionless spin magnitude of the newly formed object after the merger. The final spin is not directly measured from gravitational wave signals but is inferred using numerical relativity simulations. These are complex simulations used to solve Einstein field equations that describe the behavior of spacetime and gravitational waves in highly dynamic, strong-field regimes. These simulations are used as tool to model the merger and post-merger stages of binary systems.

Another set of parameters that extends the description (not derived from the 15) specifically for BNS is

- **Tidal distortion parameters** (Λ_1,Λ_2) - These refer to the effects of tidal forces on the shapes and orbits of the neutron stars in the binary system.

.

B. Population of events and exceptional events

By analyzing CBC events and conducting parameter estimations, we construct distributions of observed merg-

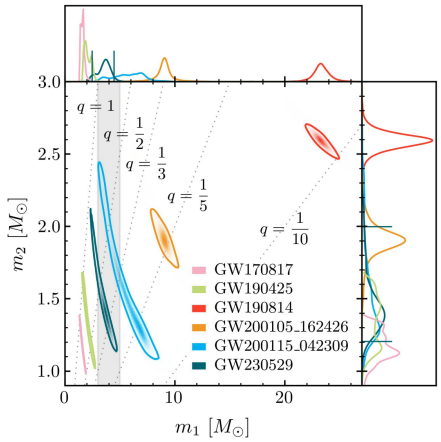

FIG. 1. Taken from [5]. The one- and two-dimensional posterior probability distributions for the Source-Frame component masses of the source binary of GW230529 (teal). The contours in the main panel denote the 90% credible regions with vertical and horizontal lines in the side panels denoting the 90% credible interval for the marginalized one-dimensional posterior distributions. Also shown are the two O3 NSBH events GW200105 162426 and GW200115 042309 (orange and blue respectively; Abbott et al. 2021a) with FAR < 0.25 yr ≈ 1 (Abbott et al. 2023a), the two confident BNS events GW170817 and GW190425 (pink and green respectively; Abbott et al. 2017a, 2019a, 2020a, 2024b), as well as GW190814 (red; Abbott et al. 2020c, 2024b) where the secondary component may be a black hole or a neutron star. Lines of constant mass ratio are indicated by dotted gray lines. The grey shaded region marks the 3–5 $M_\odot$ range of primary masses. The NSBH events and GW190814 use combined posterior samples assuming a high-spin prior analogous to those presented in this work. The BNS events use high-spin IMRPhenomPv2 NRTidal (Dietrich et al. 2019a) samples.

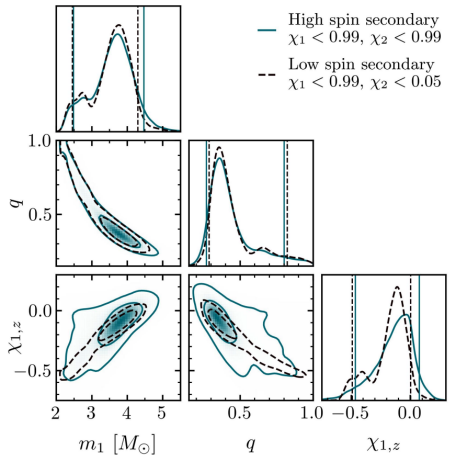

FIG. 2. Taken from [5]. Selected source properties of GW230529. The plot shows the one-dimensional (diagonal) and two-dimensional (off-diagonal) marginal posterior distributions for the primary mass m_1, the mass ratio q, and the spin component parallel to the orbital angular momentum $\chi_{1z} = \vec{\chi_1} \cdot \hat{L}$. The shaded regions denote the posterior probability with the solid (dashed) curves marking the 50% and 90% credible regions for the posteriors determined using a high spin (low spin) prior on the secondary of $\chi_2 < 0.99$ ($\chi_2 < 0.05$). The vertical lines in the one-dimensional marginal posteriors mark the 90% credible intervals.

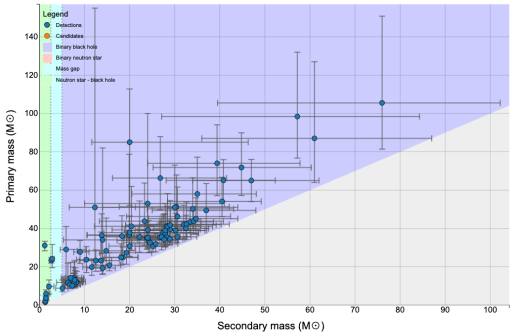

FIG. 3. Taken from [7] . Population distribution of confirmed CBC events via LIGO plotted by m_1 and m_2.

ers correcting for detectability. We then take these distributions and construct a catalog of events such as the latest Gravitational-Wave Transient Catalog (GWTC-3) [6]. From these catalogs we infer populations of events; used as the foundation for predictive models and simulations of potential future events. Populations tell us about what nature is doing, and we use observations of CBC events to infer, and gain understanding about the population of CBC events in the universe. 3 shows a distribution of events developed from confirmed CBC events observed via LIGO by the component masses m_1 and m_2. However as shown in the figure, some observed events may deviate from our distributions, termed "exceptional events". These occurrences, such as black hole mergers resulting in unusually high source-frame masses m_1, m_2, [8] or high component spins χ_1, χ_2 [9], challenge current theoretical frameworks. Presently, the origins and mechanisms behind these events are unknown. However, leading theories suggest scenarios involving hierarchical compact binary coalescence, in which coalescence binary black hole systems merge with another system [10]. A definitive understanding is lacking, leading to uncertain predictability and parameter estimation of these events, prompting our data collection and further analysis of them. Addressing this knowledge gap is crucial for advancing our comprehension of accurate estimation of astrophysical processes to further understand the evolution of black hole systems. [1].

As stated previously in section II, there exist different classes of mergers that differ from their formation mechanism such as, triple-star systems, hierarchical, dynamically captured system mergers, common evolution

systems, and many more. The measurement and understanding of exceptional events via PE, can tell us a lot about the formation mechanisms of the system in which the mergers existed in, allowing us to develop better inferences about the formation mechanisms of the population of CBC events. An example of this is in the search for evidence of dynamically captured systems. These are systems in which the black holes of a BBH pair formed independently of each other, then captured each other into an orbiting binary, usually with the help of a third object that is ejected, carrying away enough energy to leave the two heavier black holes orbitally bound. Evidence of such a merger being a dynamically captured system occurs when constructing distributions of the individual spins of the BBHs. Although the individual spins of the black holes (χ_1, χ_2) are difficult to measure, if we develop methods to measure these two parameters, in addition to the effective spin and precession of spin parameters χ_{eff}, χ_P sufficiently accurately, and measure an BBH merger event with much unaligned spins, this could serve as evidence to suggest that the BBH system was dynamically captured.

C. Parameter estimation

As stated previously given a specific GW source, such as BBH merger, PE aims to estimate the 15 parameters that characterize the event by constructing a probability posterior distribution (PPD) of where each parameter may exist. However, there lies the difficulty in visualizing all fifteen parameters. As shown in FIG 1 taken from the LVK collaboration (LIGO, VIRGO and KAGRA) visualization of data measuring the one- and two-dimensional posterior probability distributions for the component masses of the source binary of GW230529, and the one-dimensional (diagonal) and two-dimensional (off-diagonal) marginal posterior distributions for the primary mass m_1, the mass ratio q, and the spin the component parallel to the orbital angular momentum $\chi_{1z} = \vec{\chi_1} \cdot \hat{L}$ [5], scientists tend to limit the visualization to small integer dimensional analysis.

1. Methods of PE

The three main methods of parameter estimation we are focusing on in this paper are Bilby, Dingo, and GWFish. These methods employ fundamentally different methodologies. Bilby is Bayesian inference likelihood based, Dingo, Simulation based likelihood free, and GWfish, a Fisher information Matrix method.

2. Bayesian inference

Given a set of parameters $\vec{\theta}$ derived from a prior model and a set of data d, Bayesian inference aims to create a posterior distribution according to Bayes' theorem:

$$p(\theta|d) = \frac{\mathcal{L}(d|\theta)\pi(\theta)}{\mathcal{Z}}, \tag{1}$$

$p(\theta|d)$ can be interpreted as a conditional probability: the posterior probability distribution (PPD) for θ given the data d; $\mathcal{L}(d|\theta)$ is the probability of getting the data d given a set of model parameters θ. Some common assumptions are made of this function though; it is assumed that the noise is stationery and Gaussian, with zero mean. The Gaussian-noise likelihood function is:

$$\mathcal{L}(d|\theta) = \frac{1}{2\pi\sigma^2} \exp\left(-\frac{1}{2}\frac{|d-\mu(\theta)|^2}{\sigma^2}\right), \tag{2}$$

In which $\mu(\theta)$ represents an example gravitational strain waveform template derived from a given θ, σ is the detector noise, and $\pi(\theta)$ is the distribution of the prior on θ. This equation for likelihood $\mathcal{L}$ is a simplified version of the full equation, which can be derived as follows.

Given that data d is not constant but a function of time $d(t)$, we define the function of data as a combination of the signal $h(t)$ and the noise $n(t)$:

$$d(t) = h(t) + n(t). \tag{3}$$

The true gravitational wave signal in the detector is unknown, so we use signal models to describe it. These models are deemed to be a good description if the residuals $r = d - h_t$, where h_t, the matched-filter template, is an instance of the general model $\mathcal{H}$ and are consistent with the instrumental noise. Following this, simplifying assumptions, as stated previously, are made about the noise in the data $n(t)$. We can assume that the noise is Gaussian and that its probability density function (PDF) matches a uniform distribution. Using this assumption and the definitions of $d(t)$, we can now define the likelihood function as a noise model and rewrite it in the form:

$$p(d \mid h) = \frac{1}{\sqrt{\det(2\pi C)}} e^{-\frac{1}{2}\chi^2(d,h)}, \tag{4}$$

where C is the noise correlation matrix and:

$$\chi^2(d,h) = \mathbf{r}\cdot C^{-1}\cdot\mathbf{r} = (d_{I_k} - h_{I_k})C^{-1}(I_k)(J_m)(dJ_m - h_{J_m}). \tag{5}$$

Following the assumption of Gaussian noise and assuming that noise remains constant, or more specifically stationary, we can define the noise correlation matrix for each detector C to be diagonal in the Fourier domain:

$$\mathrm{S}^I_{km} = \delta_{km}\mathrm{S}^I_{(f_k)}. \tag{6}$$

We can now define $\chi^2(d,h) = (r \mid r)$, knowing that:

$$(a \mid b) = 2\int_0^\infty \frac{\tilde{a}(f)\tilde{b}^(f) + \tilde{a}^(f)\tilde{b}(f)}{S_n(f)}, df, \tag{7}$$

is a familiar inner product, in which it is understood that $S_n(f)$ represent the power spectral density also previously referred to as the detector noise σ . Given this definition, we can expand the simplified version of our likelihood function $\mathcal{L}$ and write the full function for stationary Gaussian noise that is independent in detectors as:

$$\mathcal{L}(d \mid \theta) = \exp\left(-\frac{1}{2}\sum_I \left[\int \left(\frac{(d_I - h_I(\theta))^2}{S_n^I(f)} + \ln(S_n^I(f))\right) df\right]\right) \quad (8)$$

Reverting pack to our discussion of $p(\theta|d)$, $\mathcal{Z}$ is interpreted as the integral of the numerator or normalization factor called the "evidence" [12].

$$\mathcal{Z} = \int \mathcal{L}(d|\theta)\pi(\theta)d\theta. \quad (9)$$

Although not explored in this paper, the use of evidence $\mathcal{Z}$ can be used a source of different model comparisons; this topic is explored in [13]. Given that θ is the properties of the source, the efficacy of conducting the posterior distribution is determined by the number of parameters aiming to construct distributions for, with larger numbers leading to more imprecise approximations due to correlation between the parameters. It is noted that leaving out any known parameter when conducting Bayesian Inference leads to a more inaccurate, less precise measurement. This method suffers from "the curse of dimensionality" and is computationally difficult when the source has many parameters such as CBC events. Noting the less accurate nature of the measurement, scientists often construct a **Marginalized posterior distribution** to determine the distribution for a single parameter, in which you integrate over all measures of θ_k except the one we want

$$p(\theta_i|d) = \int \left(\prod_{k\neq i} d(\theta_k)\right) p(\theta|d) \quad (10)$$

$$p(\theta_i|d) = \frac{\mathcal{L}(d|\theta_i)\pi(\theta_i)}{\mathcal{Z}}. \quad (11)$$

This equation can be written in terms of the likelihood function of the specified parameter or **marginalized likelihood function** $\mathcal{L}(d|\theta_i)$

$$\mathcal{L}(d|\theta_i) = \int \left(\prod_{k\neq i} d(\theta_k)\right) \pi(\theta_k)\mathcal{L}(d|\theta). \quad (12)$$

Marginalizing over all but one θ_i results in a 1D posterior distribution on θ_i, which contains all of the uncertainty associated with the other parameters that are covariant with θ_i. An example of this is shown in FIG 4, which shows a marginalized posterior distribution for the well-known covariance between the luminosity distance of a merging compact binary from Earth D_L and the inclination angle θ_{JN}.

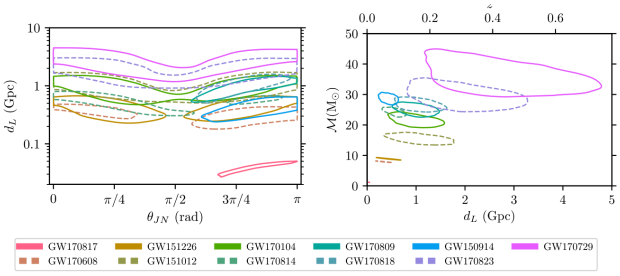

FIG. 4. Taken from [14], showing posterior probability densities of distance d_L, and inclination angle θ_{JN}

The previous most common tool used by LVK collaborations for Bayesian inference was LALInference [15]; this code is over a decade old, and and another python-toolkit has been developed using the same functionality [16]. Improvements of these methods, Bilby [17] and Dingo [18] serve as the focus of our research.

a. Bilby is a likelihood-based Bayesian Inference Python toolkit used to conduct parameter estimation. It uses sampling of a prior distribution to produce a likelihood model. This code has more versatility than its predecessors *(LALInference)*; while mostly used in the estimation of compact binary events [19, 20], it is also used in other astronomical fields such as astrophysical inference in multimessenger astronomy, pulsar timing, and x-ray observations of accreting neutron stars [17]. It serves as not only a more versatile method of Bayesian interference compared to previous methods but also boasts improvements in efficiency, speed, accuracy, and simplicity over its predecessors [17].

Bilby's development of a likelihood causes it to suffer in terms of speed compared to the other methods of PE in our study *(Dingo, Fisher Matrix)*. This is due to various things, such as the integration over multiple parameters, potential intricate relationships and non-linear dependencies among variables, complex likelihood functions that are computationally expensive to evaluate, and sufficiently large datasets. All the deficiencies get expanded with the use of advanced sampling methods such as *dynasty* [21], the nested sampling method we use in this paper to construct our PEs.

Nested sampling requires a number of live points to walk around the highest likelihood points, systematically weighting and sampling to build a posterior distribution of the parameter, and high dimensionality, complex likelihood surfaces, insufficient exploration settings, and large datasets can delay the construction of these posteriors. All this, without sufficient computational power, makes the construction of marginalized posterior distributions for singular parameters with Bilby take anywhere from hours to days, and for full fifteenth-dimensional PE, taking days to even months to complete on Bilby without the use of any additional speedup methods. Though this may be the case, Bilby is constantly in development and currently offers a multitude of settings to expedite the

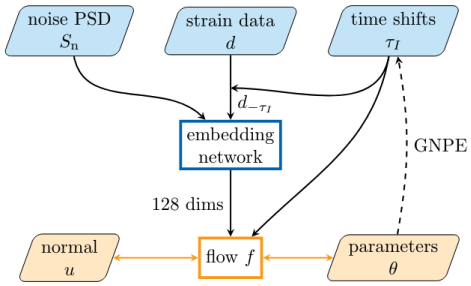

FIG. 5. Dingo flow chart taken from [18]. The posterior distribution is represented in terms of an invertible **normalizing flow** (orange), taking normally distributed random variables u into posterior samples θ. The flow itself depends on a (compressed) representation of the noise properties S_n and the data d, as well as an estimate τ_I of the coalescence time in each detector I. The data are time-shifted by τ_I to simplify the representation. For inference, the iterative *group equivariant neural posterior estimation* (GNPE) algorithm is used to provide an estimate of τ_I, as described in the main text.

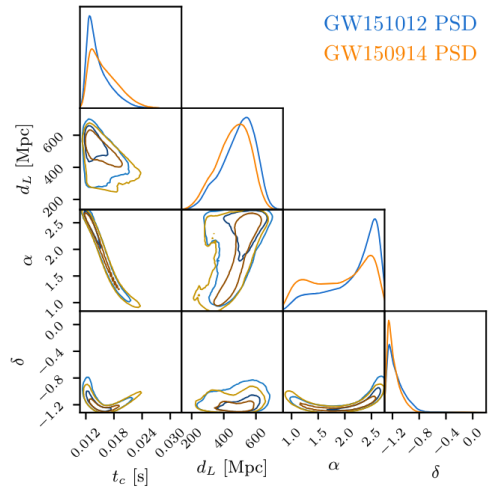

Figure 6. Comparison between DINGO evaluated on GW150914 using correct PSD as context, and using GW151012 PSD. These four parameters have a mean JSD of 0.020 nat.

FIG. 6. Taken from [18]. Comparison between Dingo evaluated on GW150914 using correct PSD as context, and using GW151012 PSD. These four parameters have a mean Jensen–Shannon divergence (JSD) of 0.020 natural information unit (nat).

process of full PE, allowing posterior distributions of confirmed detected GW signals from LIGO to be constructed within minutes of observation. Some of these advancements include *Multibanding* [22], *Relative Binning* [23], and the use of *reduced order quadratures (ROQs)* [24]. [24] and[23] delve into the latter topics more and offer a full explanation of the methods; furthermore, we shall focus on *Multibanding* and *Relative Binning* in this paper and define them later in Section III as a result of their use in our construction of posteriors and subsequent final data analysis.

b. Dingo or Deep Inference for Gravitational-wave Observations, is a likelihood-free alternative approach to Bayesian Inference. It uses artificial intelligence (AI) machine learning instead of sampling to dramatically decrease the analysis time of gravitational wave inference and parameter estimation of CBC events, at the current cost of somewhat reduced accuracy and precision. It uses the method of *neural posterior estimation* (NPE) [25, 26], in which it takes large simulated data sets with their associated parameters to train its type of neural network called a *normalizing flow* to produce a posterior distribution, generating distributions quickly after a detection is made, bypassing the need and cost of generating many waveforms at inference time [18]. A difference in how this method varies from the conventional Bayesian inference methods is how the likelihood is used. Conventional methods such as Bilby use the likelihood to determine density $p(d|\theta)$, while Dingo and NPE methods use the likelihood to simulate data $d \sim p(d|\theta)$ [18].

3. *Fisher Matrix*

A Fisher matrix or FIM (Fisher Information Matrix), approach is defined as

$$\Gamma_{\kappa\nu} = \left\langle \frac{\partial h}{(\partial\theta^k)} \middle| \frac{\partial h}{(\partial\theta^\nu)} \right\rangle = -E\left[\frac{(\partial^2 lnL)}{(\partial\theta^k \partial\theta^\nu)}\right], \qquad (13)$$

where h, following the same foundation in our equation for likelihood (8), refers to the frequency-domain strain at the detector, depending on the parameters θ^k, θ^ν. This approach assumes the waveform measured in CBC events can be seen as a linearizable approximation of the parameters, near enough to the true value, and the error distributions in the parameter errors are Gaussian, meaning the inverse of the FIM is said to give the variance-covariance matrix. Moreover, the square root of the diagonal components of the variance-covariance matrix gives an error estimation in the parameter estimation. As opposed to parameter codes that can produce multi-modal PPDs *(Bilby [17], Dingo [18])*, the FIM approach assumes a mono-modal posterior parameter distribution (PPD), assuming the 15 parameters of the observation describe a 15-dimensional space and the posterior distribution in that space is a 15-dimensional Gaussian with one peak. Rarely is this the case, as shown in both FIG 1 and 4, most events are multi-modal, consisting of multiple peaks in their distributions. Therefore, the FIM approach is only a rough, fast approximation to the most probable values of the parameters. This approach

boasts much faster speeds than Bayesian interference in parameter estimation but suffers greatly in accuracy and precision [27].

Currently there exist multiple python libraries that use this method of PE, GWFish [28], GWFast [29], and JimFisher to name a few. The method of Fisher matrix we use in this paper is GWFish.

a. GWFish is a Fisher matrix simulation software used to evaluate the current and predict the future parameter estimation capabilities of gravitational-wave detector networks. Using the Fisher matrix method, GWFish estimates errors by employing a quadratic approximation of the likelihood $\mathcal{L}$, given by:

$$\mathcal{L} \propto \exp\left(-\frac{1}{2}\Delta\theta^i \mathcal{F}_{ij} \Delta\theta^j\right), \tag{14}$$

where $\Delta\theta = \theta - \vec{\theta}$ represents the vector of parameter estimation errors, with $\vec{\theta}$ being the true parameter values. The code computes the Fisher matrix as defined in Equation (13). GWFish then calculates the covariance matrix by inverting the Fisher matrix, which represents the variance in each parameter.

One of GWFish's main strengths is its general usability, especially when compared to GWFast, which has seen much of its code deprecated. Additionally, GWFish offers more versatility than JimFisher. While JimFisher currently uses JAX [30] for automatic differentiation of waveforms, not all waveforms—especially those that include higher-order modes, such as IMRPhenomXPHM—have been implemented in JAX. Until these waveforms are supported, numerical differentiation techniques are necessary, which GWFish implements but JimFisher does not.

Moreover, the use of waveform models that account for higher-order modes significantly affects the way the Fisher matrix produces posteriors. Accounting for higher-order modes reduces the degeneracy that can occur in the posteriors, making the distribution more Gaussian. These degeneracies can manifest in various ways. An example of a well-known degeneracy between d_L and θ_{JN} was shown in Fig 4, which shows multiple peaks in the distribution. The inclusion of higher-order modes in GWFish not only decreases degeneracy in the posteriors but also constrains the variance in error estimates within the constructed posteriors. This effect is illustrated in Fig 7, which shows the difference in GWFish posterior distributions when accounting for higher-order modes in the waveform approximation versus when they are not accounted for. The usability and versatility of GWFish are the primary reasons for choosing it in our paper.

III. OBJECTIVES OF RESEARCH

Our primary goal is to conduct a comparative analysis of three parameter estimation methods—*Fisher Matrix*, *Bilby*, and *Dingo*—by employing simulated events as a benchmark, using a full spectrum of events as to assess the full capability of the models and detectors. As previously stated, we will also conduct this comparative analysis on the different methods depending on the detector being used to observe the event: *LIGO*, *Cosmic Explorer (CE)*. Furthermore, we will apply different Power Spectral Density's (PSD) to our detectors. Given the availability, we will simulate the data with a PSD of the previously observation LIGO run O3, and predictions of the PSD of observations runs O4 and O5. In which observations runs are specified time frame in which LIGO detectors are on, observing potential events, O3 marked the 3rd Ligo run and ran from 2019-2020, 04 started in 2023 and is scheduled to end in 2025, and 05 is predicted to start in 2027 lasting till 2030.

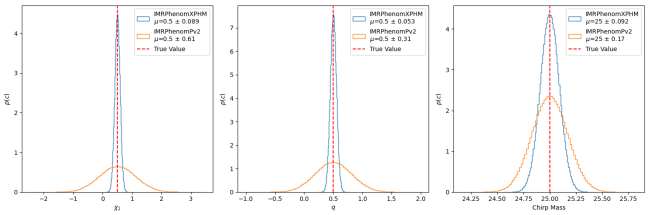

FIG. 7. GWFish posterior distributions using IMRPhenomXPHM *(blue)* and IMRPhenomPv2 *(orange)* waveform approximations for primary spin magntitude χ_1, mass ratio q, and chirp mass $\mathcal{M}$.

Another goal of this paper is to ***predict the reliability of a Fisher matrix as an accurate method of PE in future detectors (CE)***. As a Fisher matrix approach to PE assumes the 15 distributions are Gaussian, as our detectors get more sensitive, via advancements of current detectors, or construction of higher sensitive detectors e.g CE, we predict that with much higher SNRs than we currently observe, the distributions will fit a Gaussian model. Another way this can occur is as stated previously with accounting for higher-order modes in the waveform approximate model. Higher order modes limit degeneracies that cause multi-modality, the use of a model such as IMRPhenomXPHM[31] can help construct Gaussian PPDs. All of this will allow Fisher Matrix to serve as an equivalent source of accuracy and precision to other PE models, while having much higher computational speed. If our predictions are correct, this will allow PE of simulated events to be conducted much computationally faster than current standards. Though, given the predicted improvements to sensitivity, the detectors will be able to observe much farther and fainter signals than previously in which the SNR will not be high enough for a Fisher Matrix to be appropriate, in this case Bilby or Dingo will be used for PE.

Overall, this comparative study will be done by a quantitative evaluation to discern the efficacy of each method in approximating parameters of interest. In our research, we aim to measure several key aspects:

1. Speed: We will quantify the computational effi-

ciency of each method, particularly focusing on the time taken to generate parameter estimation result for events, depending and both the method and detector being used.

2. Accuracy: We will evaluate the accuracy of parameter estimations provided by each model constructed by the method. Seeing how close the average value of the estimated distributions is to the true injected parameters. This will be done using a mean calculation of the parameter distributions, and then calculating the percentage error of the known simulated parameter versus the estimated.

3. Precision: We will determine how precise each model is, examining how uniform or wide the spread of the estimated distributions are. This will be done by evaluating the standard deviation of the each of the parameter distributions, then calculating the percentage error of the known simulated parameter versus the estimated and plotting the deviation on the distribution visualization .

4. Capability: We will assess the capability of each of method of maintaining solid speed, accuracy, and precision under various conditions. This includes different degrees of deviation from the observed distribution in simulated events, the number of parameters that each model can handle, the range of parameter space it can handle, and capability between the methods via the detector being used.

5. Gausianity and Informability: We will assess how Gaussian and informative each method constructs the PPD for each parameter. This will be tested by conducting K-L divergence test comparing the constructed distributions to that of the prior, assessing how much each methods deviates from the prior.

It is to be acknowledged that each simulated event deviates from the normal distribution to varying degrees, thereby challenging the efficacy of the methods in accurately capturing these deviations. Additionally, given the intrinsic characteristics of Fisher matrices, we anticipate that although this method offers speed advantages, it will compromise on accuracy compared to other approaches. Furthermore, Dingo claims to be much faster and more efficient than the alternative Bilby [18], therefore significant increases in productivity via Dingo are expected with a caveat of a decrease in overall accuracy. It is also known that Dingo is only trained on specific simulated events, such as mass ratios from 1:1 to 1:3; it does not have the current capability to construct meaningful distributions for mass relations 1:5 or higher, therefore decreases in the capability of the model in simulated events of this variety are expected. The next-generation detector, CE [32–34], is anticipated to significantly boost the signal-to-noise ratio of observed events. As a result, all parameter estimation methods are expected to show improvements in accuracy and precision.

IV. APPROACH TO COMPARATIVE ANALYSIS

A. Simulation of waveforms

We use the ***IMRPhenomXPHM*** [31] waveform approximation to simulate our preliminary waveforms and then continue using the same frequency-domain waveform approximation subsequently. The choice to construct our waveforms from an IMR-type model instead of an effective one-body-numerical-relativity (EOBNR) model***SEOBNRv3***, or a post-Newtonian gravitational wave approximation, like Taylor approximation models [35], stems from the varying times for waveform construction between the approximation models. IMRPhenomXPHM and its subsequent successors offer faster waveform generation than other models, although with a caveat of a decrease in both accuracy and precision. We feel the level of accuracy and precision increase claimed by other models have, does not substantially change the analysis and conclusions of our data, nor does it warrant the exponentially larger waveform generation time, so we refrain from using such models.

B. Methodology of chosen injections

Given an understanding of the current distribution of CBC events, we mostly choose events that lie innately within this prior distribution, as shown in Table II.

.

TABLE II. Priors for Injection Parameters

Symbol	Distribution	Minimum	Maximum
m_1	Constraint	5	100
m_2	Constraint	5	100
q	Uniform	0.125	1
$\mathcal{M}$	Uniform	20	75
d_L	UniformSourceFrame	100	5000
δ	Cosine	-	-
α	Uniform	0	2π (periodic)
θ_{JN}	Sine	-	-
ψ	Uniform	0	π (periodic)
ϕ	Uniform	0	2π (periodic)
a_1	Uniform	0	0.99
a_2	Uniform	0	0.99
θ_1	Sine	-	-
θ_2	Sine	-	-
ϕ_{12}	Uniform	0	2π (periodic)
ϕ_{JL}	Uniform	0	2π (periodic)

We also choose "exceptional events" that lie in the outermost regions of these distributions, such as unusually high chirp masses and spins. We abstain from any PE of events below a chirp mass of $\mathcal{M} < 15$ due to Dingo's current inability to construct meaningful estimations below that threshold. Doing a combination of this allows us to "stress-test" both the models and detector capabilities, giving us not only insightful visualization insights

but also numerical insights to help build our final conclusions.

C. Use of Advancements in Models

As stated in I, Bilby offers a plethora of advancements that allow PE to speed up from taking days to mere minutes, such as relative binning, reduced order quadrature, and multibanding. The only advancement in Bilby we use in this paper for analysis is multibanding, which is defined as follows.

Multibanding Given the understanding that the inspirals of GW exist primarily at lower frequencies and that the emission of higher frequencies strongly correlates with the end of the inspiral, The technique of *MultiBanding* uses this morphology to develop waveforms at substantially lower frequencies while maintaining their accuracy. It accomplishes this by partitioning the frequency domain of the of the GW strain into bands

$$h(f) = \sum_b h_b(f). \tag{15}$$

At each band b, it evaluates the waveform at different resolutions. The bands and frequencies can be chosen based on leading post-Newtonian expressions for the time to merger as a function of frequency and chirp mass, or general error bounds for the Taylor series.

Relative Binning Heterodyning, more precisely referred to as relative binning, facilitates the integration of oscillatory functions within the waveform, particularly in likelihood construction at lower resolutions. This method operates on the assumption that waveforms supported by the posterior are similar to one another, given their alignment with the data. The technique maximizes the likelihood to select a reference waveform, $h_0(f)$, which is then used to describe any similar waveforms, $h(f : \theta)$. The reference waveform $h_0(f)$ is initially constructed at full resolution. Subsequently, smooth corrections are applied to adapt it for multiple values of θ at a lower frequency resolution. This approach allows for the frequency resolution and computational cost to remain independent of the signal's duration. As previously detailed,[23] provides a comprehensive discussion of this advanced method and the underlying process.

We refrain from using ROQs due to the fact that there is not currently an existing ROQ for CE use. The construction, or potential, of such a ROQ is currently unknown, making the use of ROQ for events detected in LIGO and the lack thereof in CE induce improper data.

D. Model enhancements and Dingo Training

Although Bilby can provide information and predictions about signals as if they were observed by CE, there is no trained Dingo network specifically for this purpose. To address this, we aimed manually train a network tailored to ensure that parameter estimation (PE) behaves as if the gravitational wave (GW) signal were observed by CE. Given that we are predicting noise levels for CE, our Dingo model was sought to be trained on a single noise realization for CE, whereas most models are trained on datasets with varying amplitude spectral densities (ASDs). This choice was driven by the lack of implementations to generate artificial noise realizations, and the uncertainty involved in assuming varying noise levels based on predictions. Consequently, we aimed to train our model on a dataset of waveform approximations constructed from **IMRPhenomXPHM**, ensuring consistency with the model used in other methods, In addition to this, the priors used in the training are those shown in Table II. Although this was our hope, we were **unable to successfully train a capability Dingo model for our project**. test toy models were constructed, but when aiming to construct a full model issues regarding waveform generation and computational expense of training hindered our attempts to successfully train a model and as such our analysis and conclusions are only based on Bilby and GWfish comparisons.

E. GWFish Prior Incorporation

GWFish currently lacks the innate implementation to incorporate priors in the sampling of its multivariate uniform distribution of parameters and construction of posteriors , which can lead to non-physical distributions such as mass ratios $q > 1$ or $q < 0$, and aligned spin magnitudes $a_i > 1$ or $a_i < 0$. This latter issue is illustrated in the Fig 7, which address the differences arising from using various waveform models, in the figure we see the distributions having a spin of less than 0 which is non physical. To incorporate priors into the distributions and fix these inaccuracies, we use two methods, but both follow the same initial process listed below.

1. Calculate the Probability Density Functions (PDFs) for Each Parameter:
For each parameter θ_i, compute the PDF $p_i(\theta_i)$ for each sample $\theta_i^{(j)}$:

$$\text{PDF}_{i,j} = p_i(\theta_i^{(j)}) \tag{16}$$

2. Compute the Product of the PDFs:
For a given set of samples $\{\theta_1^{(j)}, \theta_2^{(j)}, \ldots, \theta_N^{(j)}\}$, the product of all PDFs is:

$$P(\theta_1^{(j)}, \theta_2^{(j)}, \ldots, \theta_N^{(j)}) = \prod_{i=1}^{N} p_i(\theta_i^{(j)}) \tag{17}$$

3. Normalize the Product of PDFs:
Compute the normalization factor Z by summing the

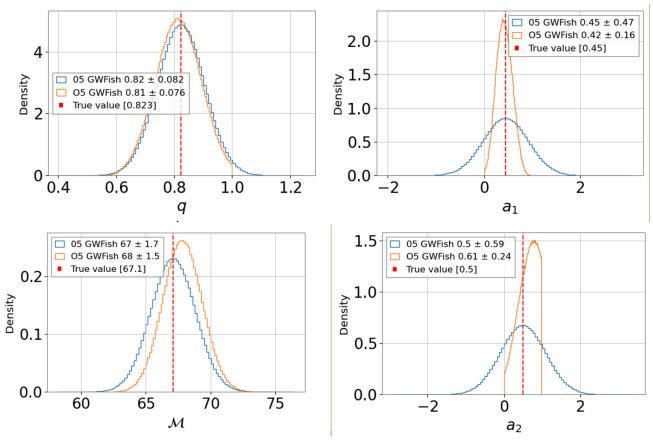

FIG. 8. Chirp mass $\mathcal{M}$, mass ratio q, and spin magnitudes a_1, a_2, posterior distributions constructed using GWFish. Blue posteriors indicated base GWFish not sampled with priors and orange shows GWFish with priors incorporated.

products of the PDFs over all samples:

$$Z = \sum_{j=1}^{M} \prod_{i=1}^{N} p_i(\theta_i^{(j)}) \tag{18}$$

Normalize the product for each sample:

$$w_j = \frac{\prod_{i=1}^{N} p_i(\theta_i^{(j)})}{Z} \tag{19}$$

where w_j is the weight associated with the j-th sample. After this, there are two approaches to incorporating priors into the distributions. First, we can use the already constructed parameter samples and simply add the weights to the graphing software used to visualize the distributions. Alternatively, we can adjust the process to incorporate priors directly into the sampling and distribution construction by

4. Resampling from the Multivariate Uniform Distribution Using the Weights:
Use the weights w_j to resample from the multivariate uniform distribution, obtaining new samples $\{\tilde{\theta}_1^{(j)}, \tilde{\theta}_2^{(j)}, \ldots, \tilde{\theta}_N^{(j)}\}$ that incorporate the prior distribution.

Following this process allows us to incorporate priors in our Fisher matrix distributions, which is needed when making comparison between the various methods of PE. The effects of using priors and lack thereof are shown in FIG 8.

F. Preliminary Comparison of Models and Detectors

We conduct preliminary stress tests on both the PE models and detectors. This is done individually for each model (*Bilby,Dingo,Fisher*) and detector (*CE,LIGO*). This is implemented by manually choosing injections that lie within a known prior distribution of BBH events, simulating them with the ***IMRPhenomXPHM*** waveform approximation, then feeding the waveform to our detectors and conducting PE with our methods. Next, we construct corner plots similar to those shown in FIG. 2 of the desired parameters. Though an understanding of all 15 parameters will be numerically understood, for our test, we focus on and visualize only "intrinsic parameters". These are of importance because some of these parameters greatly affect the structure of the waveform, e.g., chirp mass $\mathcal{M}$ and effective spin χ_{eff}, which are more easily observed than parameters such as the individual spin of a BH χ_1, giving us better insight as a whole from the PE. After initial visualization, we build a table of all 15 estimated parameter distributions. The table has rows of the parameters and columns of time taken to generate PE, means of distributions, standard deviation, true value of parameters, accuracy's, calculated from the percent error of the mean, and precision's, calculated from the percent error of the standard deviation.

1. *Comparison via different detectors:*

LIGO currently has two detectors, one in Hanford, Washington, and the other in Livingston, Louisiana. Their respective, known performance is well documented, with their capability and spectral noise curve both respectively known [1, 5, 8–10, 15–20, 25, 26, 36]. CE is a next-generation observatory concept that will greatly deepen and clarify humanity's gravitational-wave view of the cosmos. It will have an L-shaped geometry and house a single interferometer. The CE facility will have two 40 km ultrahigh-vacuum beam tubes, roughly 1 m in diameter, and two 40 km arms that are 10 times longer than Advanced LIGO, resulting in high increases in the signal-to-noise ratio for any given source. Being built with all new technology based upon current LIGO technology, the observatory will offer increases in sensitivity and bandwidth of the instruments [32–34].

Estimating the improvement in observations via CE, we have simulated data as if it were detected by the observatory using both Bilby's and Gwfish's innate CE configuration settings, looking for events at much lower frequencies than LIGO has the means to detect. We have then simulated the same event for the current LIGO observatories and conduct parameter estimation on these events via both methods, following the same format as explained previously. Doing this allows us to show the improvement of parameter estimation via the technological advancements of detectors and offer insight into the changes in efficiency and capability of each parameter estimation method due to different detectors.

Following the initial test, we inject the same parameters using the same waveform approximation model but using a different PSD for the detectors. Following the same format as the initial test, we visualize important

parameters and build a table using the same format as previously described. Next, we conduct comparisons between the different developed posteriors visually by constructing overlapping histograms of specific intrinsic parameters, constructing a table in the same format as before but with both estimation values and errors. We then numerically take both the numerical values and percent error values of accuracy and precision and compare the two PEs in totality.

2. *Exceptional Events*

After preliminary data collection, model visualization, and numerical data comparison, we then simulate multiple high-mass, exceptional black hole merger events. After manually injecting a high mass and event into our waveform approximation, we then use both methods for PE. Using the same format as the initial preliminary comparison to avoid errors, we conduct parameter estimation using each method, visualize specific parameters, construct tables of distribution values, repeat for varying PSD scenarios, visualize and compare the different PEs, and finally numerically compare the different methods.

G. Further comparisons between models and detectors

Using injected data, we conduct a qualitative and quantitative comparative analysis of all methods, looking at the methods together and delineating where the strengths and weaknesses lie within each. Given our preliminary comparisons and stress tests of models and detectors, we then follow the same format as the preliminary comparison for further analysis, but instead of individually looking at specific combinations of models and detectors and measuring the degree of difference in the approximation to that of the simulated distribution, as stated previously, we combine analysis for both methods of PE. We then construct histograms comparing the distributions formed from specific parameters from each method and model, construct tables in the same format delineating accuracy, precision, and speed, numerically define the overall effectiveness of each method by using a comparison of the values in the table, and use said data to offer predictions on how this effectiveness may shift in the future.

V. DATA ANALYSIS

A. Preliminary Tests

All preliminary tests are developed using the injected parameters shown in Table III.

TABLE III. Injected Parameters for Preliminary Tests

Symbol	Test 1	Test 2	Test 3	Test 4	Test 5
m_1	36.0	40	40	85.0	85.0
m_2	29.0	25	25	70.0	70.0
q	0.805	0.625	0.625	0.823	0.823
$\mathcal{M}$	28	27.38	27.38	67.1	67.1
d_L	1000.0	4000.0	1000.0	4000.0	1000.0
δ	-1.2	0.6	0.6	0.6	0.6
α	1.375	4.307	4.307	4.307	4.307
θ_{jn}	0.4	2.0	2.0	0.6	2.0
ψ	2.659	3.0	3.0	3.0	3.0
ϕ	1.3	4.5	4.5	4.5	4.5
a_1	0.4	0.4	0.8	0.8	0.45
a_2	0.3	0.5	0.2	0.2	0.5
θ_1	0.5	2.5	2.7	2.7	2.5
θ_2	1.0	3.8	3.8	1.5	2.5
ϕ_{12}	1.7	5.5	5.5	5.5	5.5
ϕ_{jl}	0.3	5.2	5.2	3.892	5.3
t_c	1126259642.413	-	-	-	-

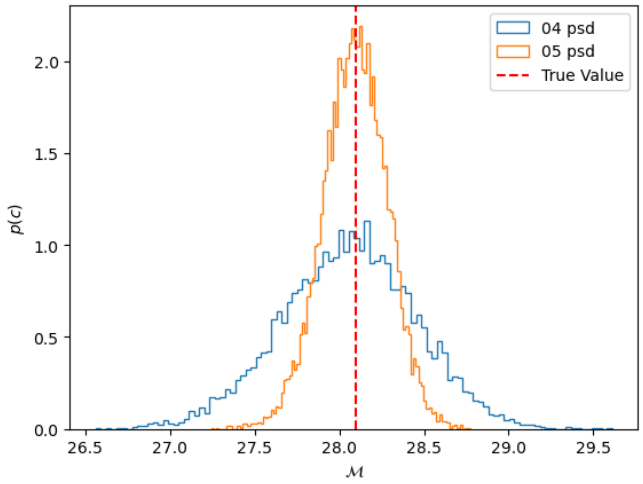

FIG. 9. Comparison of chirp mass $\mathcal{M}$ PPDs for o4 *(blue)* and o5 *(orange)* PSD predictions. Constructed using Bilby and injection parameters from Test 1.

1. *Fisher Matrix Test*

Using the injections listed in Table III, we will initially address our impressions of the method before discussing the results. Given our aim of trying to determine to what extent is a Fisher matrix a reliable source of PE, the test are conducted using O5 and CE noise realizations, this is because we expect at these low noise levels the true distributions of the parameters are going to be more Gaussian distributed in Bilby, than in 04 detections. Given that a Fisher matrix assumes this, only at these high nose levels is a comparison with Bilby and GWfish meaningful.

Although GWfish is the best option for Fisher matrix PE for our study, it still has some inadequacies. One such inadequacy, previously mentioned in Section IV, is GWfish's lack of innate implementation for incorporating priors in constructing distributions. This limitation signifi-

cantly hindered the speed at which these tests could be conducted, as comparing and understanding results from incorporating priors and the base GWfish was necessary to gauge the overall efficiency of the method. Despite this issue, GWfish does offer a more streamlined process for Fisher matrix construction and distribution development compared to other software. This allowed for relatively easy and straightforward manual adaptation of the software in comparison with other Fisher matrix software.

Following these initial impressions, the preliminary tests showed the following results using CE and current GW detectors (LIGO):

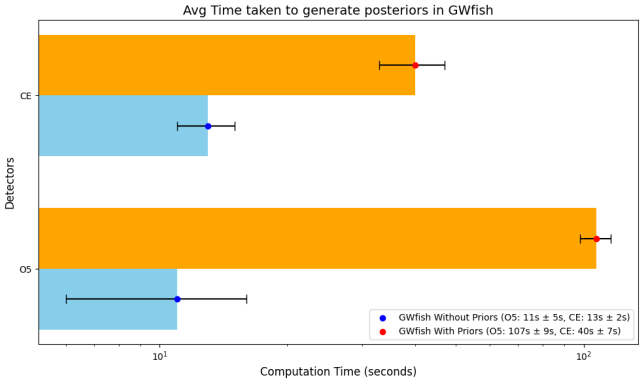

FIG. 10. Time in seconds s, taken by GWfish to generate posteriors from 10^9 samples, depending on detector *(O5,CE)*, with priors (*orange*), and without priors (*blue*)

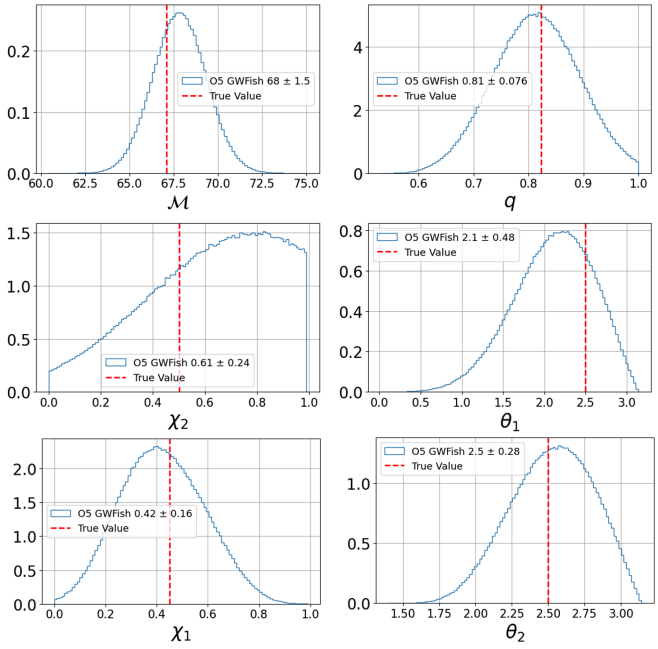

FIG. 11. GWfish posterior distributions for chirp mass ($\mathcal{M}$), mass ratio (q), component spins (χ_1, χ_2), and tilt angles (θ_1, θ_2) using O5 predicted noise levels.

Speed: Without incorporating priors, using the five stated injections in Table III, as shown Fig 10 GWfish took approximately 11 ± 5 and 13 ± 2 seconds to construct distributions after each injection for O5 and CE respectively. With the incorporation of priors, due to the need to resample with new weights, the speed of GWfish posterior construction decreased to 107 ± 9 seconds for O5 and 40 ± 7 seconds for CE. Although accuracy and precision statistics were not collected for GWfish without priors (as the results were non-physical), it is still valuable to provide a reference for the average time GWfish requires to compute base distributions. The observed reduction in computation time for CE compared to current LIGO detectors can be attributed to several factors. One possibility is that since CE will produce higher-quality data with less noise, this means that the initial sampling of the posteriors results in more samples fitting within the prior distributions, allowing for faster sampling when incorporating priors, as opposed to LIGO posteriors, which contain many non-physical samples. These non-physical samples increase the computational time required, explaining the difference when compared to CE.

Accuracy: A Fisher matrix by its nature is going to have high accuracy with its assumption of the shape of the distribution, visualizing specific intrinsic parameters in FIG 11, we observe this expected accuracy. Focusing on the spin magnitudes χ_1 and χ_2, we see that in O5 events, the samples constructed with GWfish are not well-constrained, often resulting in nonphysical distributions. After applying priors and truncating the data, the overall accuracy of these parameters decreases, with the mean of the distribution shifting away from the true value. However examining the same event in CE, which results in higher SNR, leads to more constrained signals, therefore distributions do not exhibit the shift in distribution shown in the O5 results. Instead, as shown in FIG 12, they are completely Gaussian distributed, centered at the true value. This trend is consistent across all simulated events, and the overall accuracy appears promising and aligned with the expectations based on the Fisher matrix formalism.

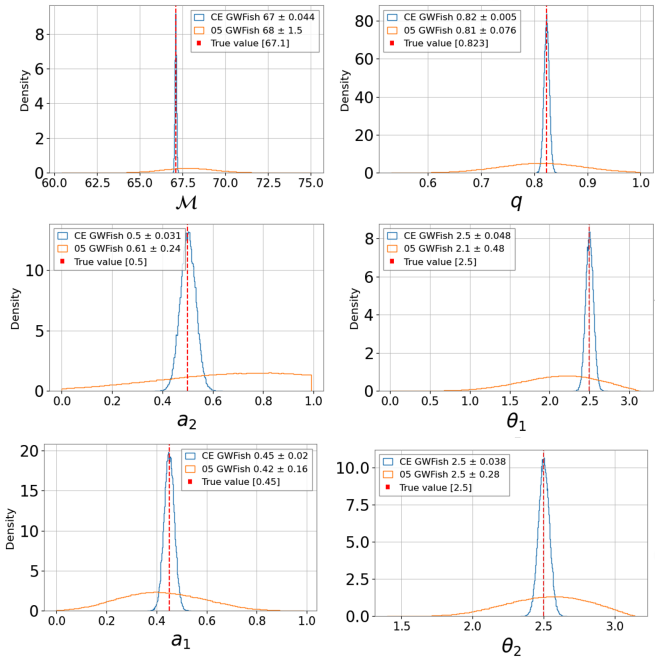

FIG. 12. GWfish posterior distributions for chirp mass ($\mathcal{M}$), mass ratio (q), component spins (a_1, a_2), and tilt angles (θ_1, θ_2) using O5 *(orange)* and CE *(blue)*predicted noise levels.

Precision: Also shown in FIG 12, the overall precision of the CE and O5 GWfish results met expectations. The 05 results demonstrated high precision, characterized by narrow distributions. However, consistent with the trend observed for accuracy, the CE results showed a significant increase in precision compared to O5. For all comparable intrinsic parameters, the CE distributions were much more tightly constrained, with small deviations from the overall mean.

Quantitatively, it was observed that CE results were, on average, over 50% more precise than O5 results. Parameters related to individual tilt angles, θ_1 and θ_2, showed the most dramatic improvements in precision, with increases of approximately 75% and 80%, respectively.

Given than the SNR signal for O5 events fluctuating in the 10s, while CE SNR are in the 100s, the overall level of precision increase does make sense, and fall in line with what we expected of method.

2. *Bilby Tests*

For the Bilby test, we used the injections shown in Table III, constructing distributions using data from O4, O5, and CE. Similar to the Fisher matrix test, we will first provide our overall impressions of the method, followed by a comparison of the results across the different detectors.

Bilby stands out as the most intuitive and user-friendly method of PE discussed in this paper. Compared to other methods, Bilby offers the most convenient and effective framework for PE. As the current standard in gravitational-wave PE this ensures that it is well-documented and regularly updated. This ease of use and ongoing development gives Bilby a distinct advantage over newer methods like Dingo and GWfish, which are still evolving in terms of both functionality and user support.

The results of our Bilby tests for O4 O5 and CE test are as follows:

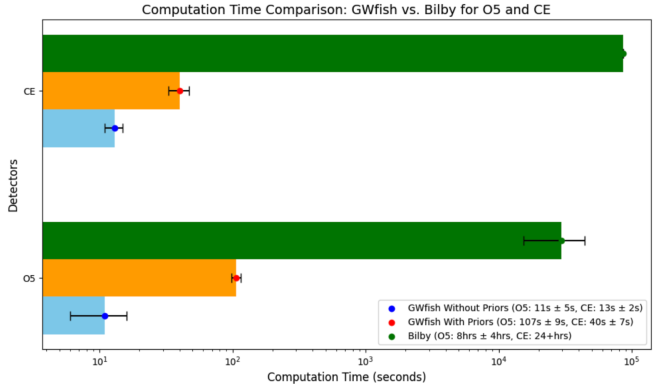

FIG. 13. Comparison between time taken in seconds s to generate posteriors for each detector *(O5,CE)* in Bilby *(green)*, GWfish with priors (*orange*), and without priors (*blue*).

Speed: Bilby's primary limitation in parameter estimation (PE) is its computational speed for O4, O5, and CE detections. Referring to FIG 13, for the same injections used in GWfish PE for current LIGO detectors, Bilby took an average of 8–8.5 hours to construct distributions. For Cosmic Explorer (CE), this time dramatically increased to over 24 hours to generate distributions. In contrast to GWfish, the increased computational expense for Bilby in CE detections stems from its likelihood-based approach. Since CE signals contain significantly less noise, the resulting distributions are much more constrained, which makes the likelihood steeper and more challenging for Bilby's sampling algorithms to handle. However, Bilby's computational burden was reduced by several hours with the use of techniques like relative binning and multibanding. Despite these improvements, due to its likelihood-based nature, Bilby will always remain computationally expensive when dealing with highly constrained distributions, especially in the context of CE detections.

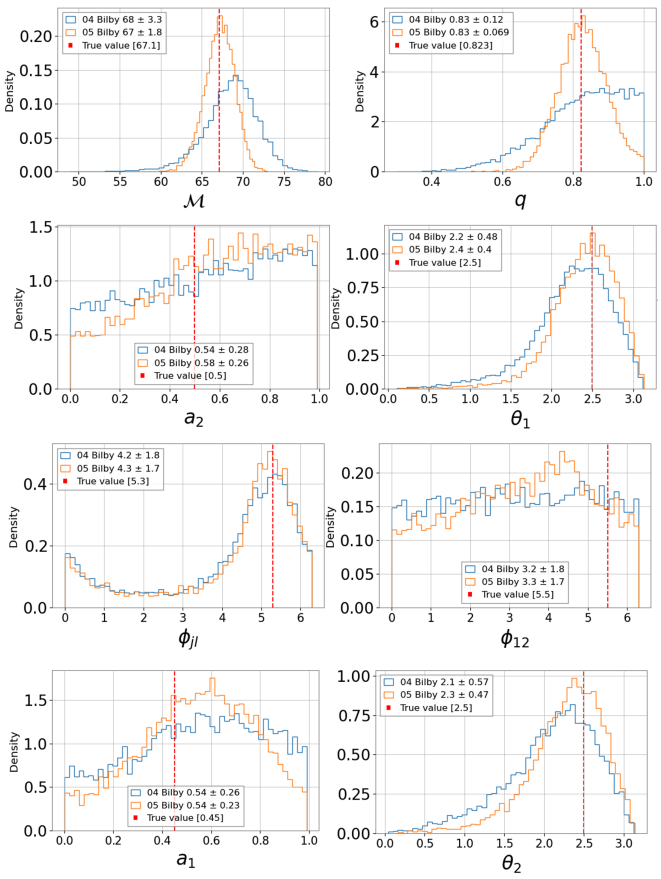

FIG. 14. Bilby posterior distributions for chirp mass ($\mathcal{M}$), mass ratio (q), component spins (a_1, a_2),and spin angles ($\theta_1, \theta_2, \phi_{jl}, \phi_{12}$) using O5 *(orange)* and O4 *(blue)*predicted noise levels.

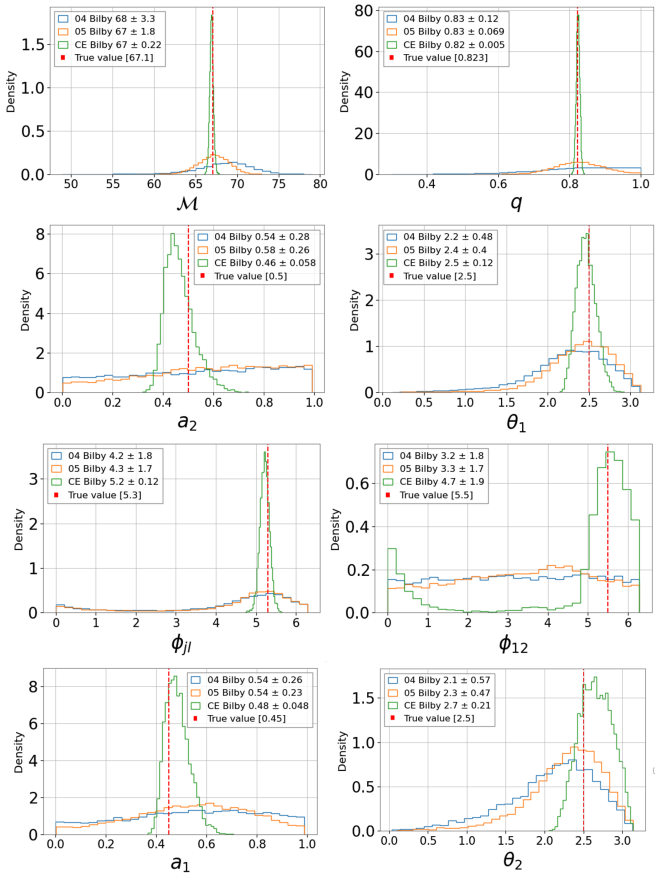

FIG. 15. Bilby posterior distributions for chirp mass ($\mathcal{M}$), mass ratio (q), component spins (a_1, a_2), and spin angles ($\theta_1, \theta_2, \phi_{jl}, \phi_{12}$) using O4 *(blue)*,O5 *(orange)*, and CE *(green)* predicted noise levels.

Accuracy: As shown in FIG 14, Bilby estimated accurate distributions for specific intrinsic parameters such as the chirp mass ($\mathcal{M}$), mass ratio (q), and the tilt angles (θ_1, θ_2) for both O4 and O5 detections. In particular, Bilby also displayed notable accuracy in estimating the highly degenerate parameter ϕ_{JL}. Although the accuracy of all parameters improved in O5 compared to O4, Bilby continued to face challenges in constraining more complex parameters such as the precession angle ϕ_{12}, and the spin magnitudes χ_1 and χ_2, which are inherently more difficult to measure due to their weak coupling to the observed gravitational-wave signal.

When comparing these results to Cosmic Explorer (CE) data, as shown in FIG 15, we observed a dramatic improvement in the accuracy of all parameters. Even the parameters that were difficult to constrain in O4 and O5 are measured with significantly greater accuracy in CE. This is particularly impressive considering the highly degenerate and uncertain nature of parameters like ϕ_{12} and the spins χ_1 and χ_2, which are now accurately estimated in CE due to the increased signal-to-noise ratio (SNR) and the improved sensitivity of CE. Quantitatively, while Bilby's accuracy for O4 and O5 detections ranged between 60% and 86%, depending on the parameter, CE exhibited accuracy rates between 79% and 92% across all parameters. This dramatic increase in accuracy, coupled with the overall narrowing of the uncertainty in these measurements, highlights the potential of CE to fully constrain the intrinsic parameters of gravitational wave events.

Precision: Referring back to FIG 14,we see both O4 and O5 detections, Bilby demonstrated increasing levels of precision, with the distributions becoming more Gaussian-shaped as the data improved. Similar to the trends seen in accuracy, the intrinsic parameters that are easier to measure—such as the chirp mass ($\mathcal{M}$), mass ratio (q), and tilt angles (θ_1, θ_2)—produced the most precise distributions for both O4 and O5. These parameters exhibited well-constrained, narrow distributions, reflecting their more straightforward detectability in gravitational-wave signals. However, for other, more challenging parameters, the precision fluctuated greatly. In some cases, the distributions closely followed the priors, showing little resemblance to a Gaussian shape and showing the difficulties in constraining these parameters. This lack of precision, particularly in parameters like the spin components and precession angles, indicates the lim-

itations of current LIGO detectors (O4 and O5) when it comes to measuring complex or degenerate quantities. As expected, in the case of Cosmic Explorer (CE), the precision dramatically improved across the board. As shown in Fig 15, CE produced much more tightly constrained distributions, with nearly all parameters exhibiting Gaussian-like shapes symmetrically distributed around the true values. This marked improvement in precision extended to all intrinsic parameters analyzed, including those that were previously difficult to measure with high accuracy, such as spin magnitudes and precession angles.

Quantitatively, it was found that while the precision of distributions for O4 and O5 detections ranged from 40% to 75%, CE demonstrated precision ranging from 78% to 95%. This significant leap in precision underscores the potential of CE to provide highly reliable parameter estimates for a wide range of gravitational-wave events. The narrower, Gaussian-shaped distributions indicate that CE will be able to offer much more consistent and accurate measurements of the intrinsic properties of binary systems, even for parameters that are notoriously difficult to constrain with current detectors.

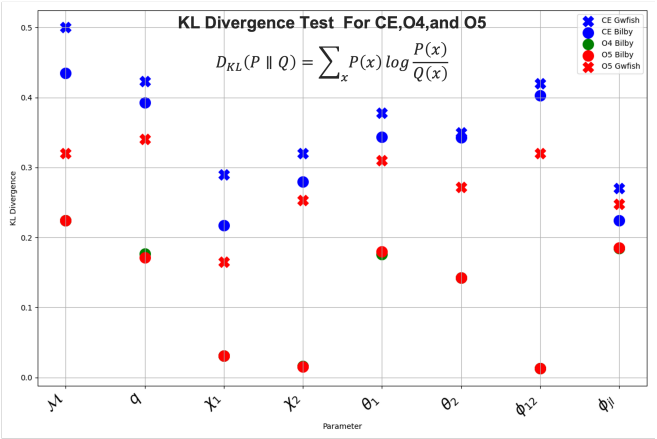

FIG. 16. Kullback–Leibler divergence with respect to priors for distributions of mass ratio q, chirp mass $\mathcal{M}$, individual component spins χ_1, χ_2, and spin angles $\theta_1, \theta_2, \phi_{jl}, \phi_{12}$. The plot shows results for GWFish (diamonds) and Bilby (circles). Noise predictions for O4 are indicated in green, O5 in red, and CE in blue.

B. GWFish Bilby Comparisons

When comparing the data obtained from Bilby and GWfish for drawing conclusions about GWfish's overall capability, it is essential to focus on specific parameters of interest. These parameters fall into categories based on two main criteria in the Bilby data: they must be highly accurate, deviating very little from the true value, and they must be highly precise, exhibiting distributions that resemble a nearly Gaussian shape.

As shown in FIG 17, the only parameters that meet these criteria for O4 and O5 distributions are the chirp mass ($\mathcal{M}$), mass ratio ($q < 1$), and the precession parameter (ϕ_{JL}). When we compare these Bilby distributions to those generated by GWfish, as seen in the figure, the Bilby results closely resemble the GWfish posteriors for each of the specified parameters. This serves as potential evidence that for these particular parameters, GWfish may be capable of accurately estimating these intrinsic properties. The fact that both methods produce similar distributions suggests that GWfish potentially be trusted for these specific parameters, even with the differences in underlying methodology.

This trend also holds true for CE data, with the addition of the tilt angle parameter θ_1 meeting the accuracy and precision criteria, as shown in FIG 18 and 19 . When comparing these CE results from Bilby to GWfish, we observe that the distributions almost completely overlap, with only minor deviations in the mean of the distributions. This provides even stronger evidence that, at higher signal-to-noise ratios (SNRs), GWfish could serve as a reliable and efficient method for parameter estimation for these parameters. Although the figure illustrates the results for one event, these parameters consistently meet the accuracy and precision criteria across all conducted tests. This consistency reinforces the potential of GWfish as a fast and reliable tool for future PE, especially when focusing on parameters $\mathcal{M}$, q, ϕ_{JL}, and θ_1 at high signal-to-noise ratios (SNRs).

Another key point of evidence supporting GWfish's reliability comes from testing the informativeness and Gaussianity of the distributions. Using the method described in Section II, we performed K-L divergence tests to compare the priors to the constructed distributions. These tests show how much the posterior distributions deviate from their priors and how informative and Gaussian-like they are. Shown in FIG 16, for current LIGO detectors (O4 and O5), the K-L divergences are relatively low for most parameters, indicating that the posteriors deviate minimally from the priors, meaning the distributions are less informative and less Gaussian. However, when examining the K-L divergences for CE data, we observe significantly higher divergences across all intrinsic parameters, indicating that the CE posteriors are much more informative. Of particular interest is the close match between the K-L divergences for GWfish and Bilby in CE events. For the parameters of interest—$\mathcal{M}$, q, ϕ_{JL}, and θ_1—the K-L divergences between GWfish and Bilby are quite similar, indicating that the distributions for these parameters are closely aligned between the two methods. This provides further evidence that, for high SNR events, Bilby's distributions resemble those generated by a Fisher matrix approach (as used in GWfish). Thus, GWfish could be a reliable and efficient alternative for parameter estimation in high SNR scenarios.

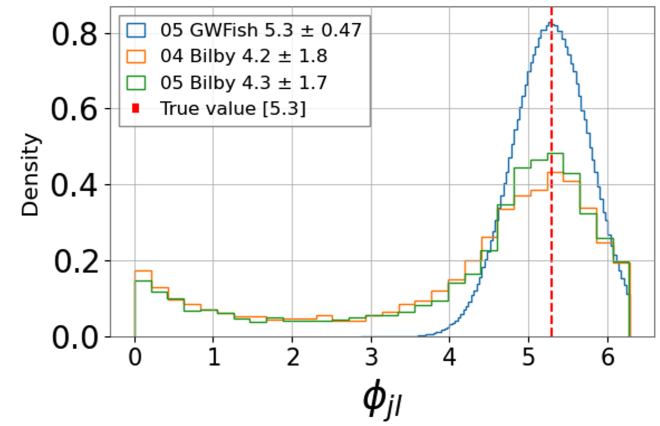

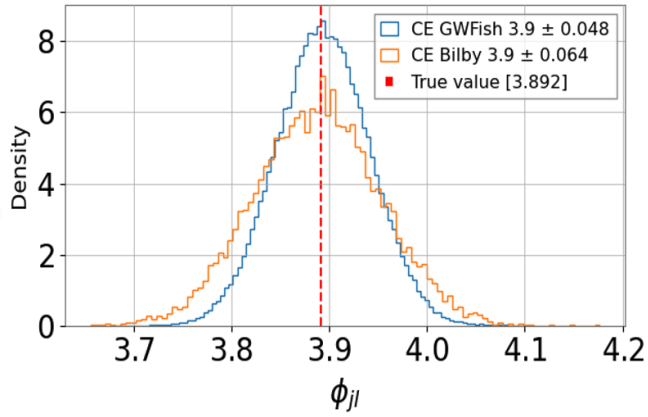

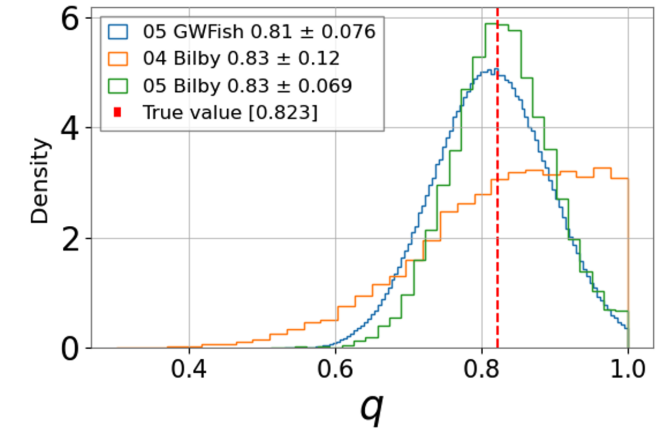

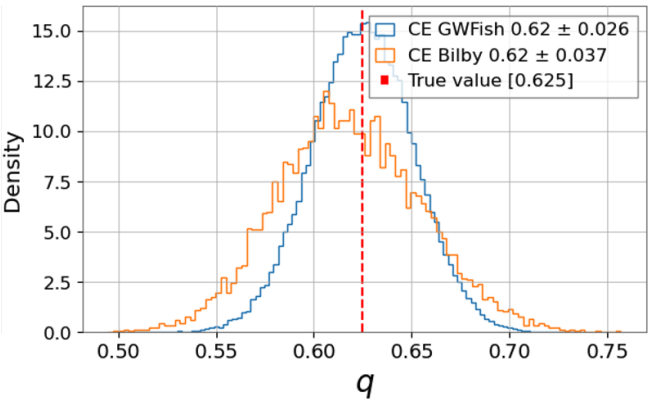

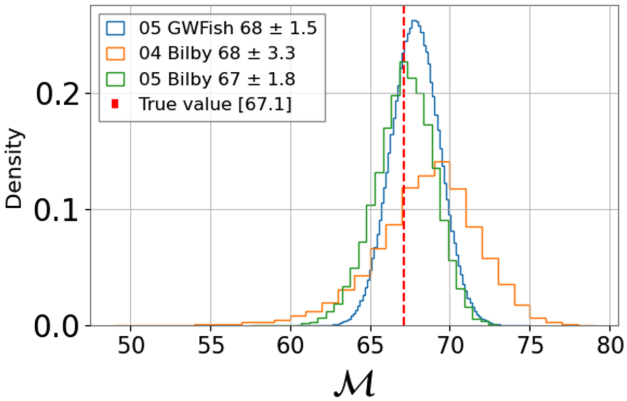

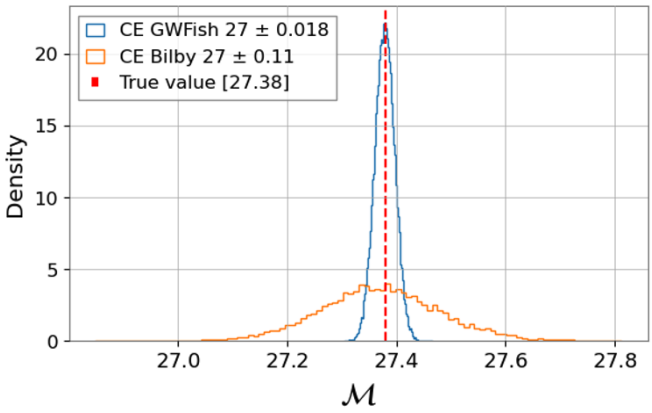

FIG. 17. Comparisons between constructed distributions for spin angle ϕ_{jl}, mass ratio q, and Chirp mass $\mathcal{M}$, using O5 noise predictions for GWFish *(blue)*, and O4 (orange) O5 (green) noise predictions for Bilby.

FIG. 18. Comparisons between constructed distributions for spin angle ϕ_{jl}, mass ratio q, and Chirp mass $\mathcal{M}$, using CE noise predictions for GWFish *(blue)*, and Bilby *(orange)*.

VI. CONCLUSIONS

In our study we have provided evidence showing that Cosmic Explorer (CE) is expected to exhibit dramatic increases in capability and reliability compared to LIGO detectors. Our data shows that CE provides an average increase of 25% in accuracy and over a 30% increase in precision compared to O4 and O5 detections. However, while CE significantly enhances accuracy and precision, it comes with a notable trade-off in terms of computational speed, especially when using Bilby. CE events take considerably longer to process compared to O4 and O5, highlighting the need for further developments to speed up posterior construction. One promising approach is the development of Reduced Order Quadratures (ROQs)

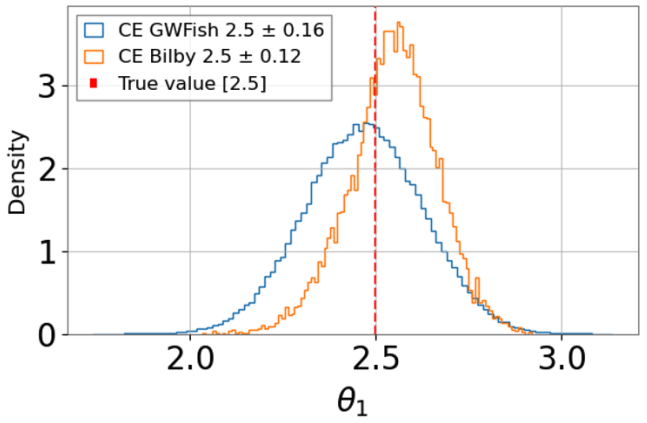

FIG. 19. Comparisons between constructed distributions for primary spin tilt angle θ_1, using CE noise predictions for GWFish *(blue)* and Bilby *(orange)*.

specifically for CE, which have not yet been fully developed. Additionally, for current LIGO detectors, we found that due to the non-Gaussian nature of the constructed likelihood posteriors, it is unlikely that a Fisher matrix method could serve as a reliable source of parameter estimation (PE) for these events. However, for CE detections, we have shown that for specific intrinsic parameters—$\mathcal{M}$, q, ϕ_{JL}, and θ_1—there is evidence to suggest that, given the shape and accuracy of Bilby's distributions, a Fisher matrix method could be a reliable and efficient tool for PE in these high-SNR events. Given the preliminary nature of our work, only tentative conclusions can be drawn at this time, with plans to provide more definitive results and further insights in future studies.

VII. FUTURE WORK

To provide more definitive answers and build upon this study, we plan to explore several avenues for future research. Firstly, to comprehensively compare the three types of PE methods discussed in this paper, we intend to develop a capable Dingo model able to make detections with CE noise realizations. We will then run the same injections used in this study with the Dingo model and compare the results to those obtained with the existing Dingo distributions. Next, we aim to expand our comparisons in a multifaceted manner. Specifically, we plan to assess the reliability of Fisher matrix methods by delineating events based on specific signal-to-noise ratios (SNRs) and frequencies. Given that GWfish appears reliable at high SNRs, our goal is to determine the numerical range of SNRs where GWfish and other Fisher matrix methods become reliable sources of PE. This will help to better understand the conditions under which these methods perform optimally. Additionally, we will use a broader variety and overall greater quantity of injections to explore different types of events. This will provide a more comprehensive analysis of the methods' performance across various scenarios. We also plan to conduct comparisons using different priors. Currently, we have used a singular default non-astrophysical prior, but we will incorporate astrophysical priors in future studies and compare the results to those obtained with the non-astrophysical prior. Lastly, as addressed in the sections on LIGO and CE, these detectors are not singular entities but rather collections of individual detectors. Therefore, as shown in FIG 20, we could perform comparisons as if the events were detected by each individual component of the various detectors, allowing for a more detailed analysis. In summary, this study serves as solid preliminary work and has laid the foundation for our future work in the comparison of PE methods.

VIII. ACKNOWLEDGEMENTS

This work was supported by the National Science Foundation Research Experience for Undergraduates (NSF REU) program, the LIGO Laboratory Summer Undergraduate Research Fellowship program (NSF LIGO), and the California Institute of Technology Student-Faculty Programs.

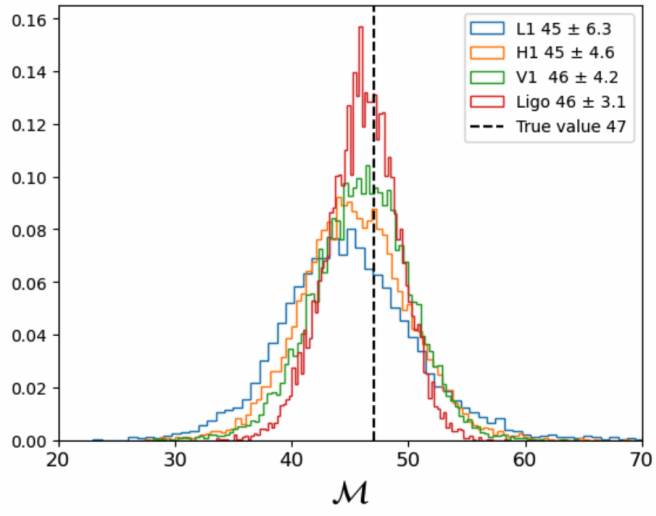

FIG. 20. Example distributions for Chirp Mass $\mathcal{M}$, found by conducting PE individually for each Ligo detector.

Parameter	Avg Accuracy ± Std Accuracy	Avg Precision ± Std Precision
m_1	0.83 (2.2%) ± 0.71 (2.4%)	3.2 (8.3%) ± 1.7 (6.2%)
m_2	1.4 (3.3%) ± 1.9 (5.0%)	4.4 (10.0%) ± 2.9 (8.3%)
d_L	560 (42%) ± 1100 (94%)	420 (14.0%) ± 570 (11.0%)
θ_{jn}	0.15 (19.0%) ± 0.16 (32.0%)	0.2 (18.0%) ± 0.09 (11.0%)
δ	0.039 (5.7%) ± 0.054 (9.4%)	0.093 (13.0%) ± 0.082 (20.0%)
α	0.056 (1.6%) ± 0.068 (1.7%)	0.11 (3.6%) ± 0.09 (3.4%)
ψ	0.15 (5.1%) ± 0.2 (7.2%)	0.19 (7.6%) ± 0.16 (8.5%)
ϕ	0.31 (11.0%) ± 0.38 (23.0%)	0.52 (15.0%) ± 0.36 (14.0%)
χ_1	0.13 (24.0%) ± 0.1 (21.0%)	0.18 (38.0%) ± 0.054 (17.0%)
χ_2	0.14 (52.0%) ± 0.11 (52.0%)	0.19 (47.0%) ± 0.071 (13.0%)
θ_1	0.49 (30.0%) ± 0.38 (39.0%)	0.4 (26.0%) ± 0.16 (15.0%)
θ_2	0.45 (21.0%) ± 0.39 (13.0%)	0.37 (22.0%) ± 0.17 (11.0%)
ϕ_{12}	1.0 (24.0%) ± 1.0 (25.0%)	1.1 (33.0%) ± 0.27 (19.0%)
ϕ_{jl}	0.24 (29.0%) ± 0.27 (77.0%)	0.6 (26.0%) ± 0.32 (23.0%)

TABLE V. Table of accuracy and precision metrics of Fisher Matrix preliminary test 1 for current LIGO detectors, showing the average values ± standard deviations, including percentage values.

IX. APPENDIX A

Parameter	Avg Accuracy ± Std Dev	Avg Precision ± Std Dev
m_1	0.15 (0.31%) ± 0.21 (0.51%)	0.68 (1.3%) ± 0.51 (1.2%)
m_2	0.10 (0.31%) ± 0.15 (0.58%)	0.46 (1.3%) ± 0.36 (1.3%)
d_L	870 (74%) ± 1500 (140%)	410 (13%) ± 550 (12%)
θ_{jn}	0.018 (2.6%) ± 0.032 (6.4%)	0.052 (5.9%) ± 0.049 (6.8%)
δ	0.20 (14%) ± 0.28 (41%)	0.11 (1.5%) ± 0.12 (26%)
α	0.24 (10%) ± 0.32 (20%)	0.14 (10%) ± 0.13 (22%)
ψ	0.35 (12%) ± 0.40 (15%)	0.24 (11%) ± 0.15 (8.5%)
ϕ	0.13 (3.4%) ± 0.16 (3.7%)	0.30 (11%) ± 0.23 (14%)
χ_1	0.019 (4.2%) ± 0.046 (12%)	0.034 (6.1%) ± 0.029 (6.0%)
χ_2	0.028 (10%) ± 0.041 (15%)	0.069 (22%) ± 0.051 (16%)
θ_1	0.025 (1.2%) ± 0.043 (1.7%)	0.070 (5.4%) ± 0.057 (7.6%)
θ_2	0.12 (5.4%) ± 0.25 (8.4%)	0.16 (9.5%) ± 0.18 (11%)
ϕ_{12}	0.037 (0.75%) ± 0.073 (1.3%)	0.25 (6.9%) ± 0.12 (6.0%)
ϕ_{jl}	0.056 (5.7%) ± 0.084 (19%)	0.13 (9.2%) ± 0.14 (14%)

TABLE IV. Table of accuracy and precision metrics of Fisher Matrix preliminary test 1 for future detectors (CE), showing the average values ± standard deviations, including percentage values, for all parameters.

[1] M. Spera, A. A. Trani, and M. Mencagli, *Compact Binary Coalescences: Astrophysical Processes and Lessons Learned*, Galaxies **10**, 10.3390/galaxies10040076 (2022).

[2] D. R. Czavalinga, T. Mitnyan, S. A. Rappaport, *et al.*, *New compact hierarchical triple system candidates identified using Gaia DR3*, Astronomy & amp; Astrophysics **670**, 10.1051/0004-6361/202245300 (2023).

[3] B. P. Abbott, R. Abbott, T. D. Abbott, *et al.*, *GW190425: Observation of a Compact Binary Coalescence with Total Mass ≈ 3.4 M⊙*, The Astrophysical Journal Letters **892**, L3 (2020).

[4] A. Fabio, T. Silvia, and A. S. Hamers, *Binary Black Hole Mergers from Field Triples: Properties, Rates, and the Impact of Stellar Evolution*, The Astrophysical Journal **841**, 77 (2017).

[5] The LIGO Scientific Collaboration, Virgo Collaboration, and the KAGRA Collaboration, *Observation of Gravitational Waves from the Coalescence of a* 2.5 − 4.5 $M_\odot$ *Compact Object and a Neutron Star* (2024), arXiv:2404.04248 [astro-ph.HE].

[6] .

[7] https://catalog.cardiffgravity.org,.

[8] B. P. Abbott *et al.* (LIGO Scientific Collaboration and Virgo Collaboration), *GW190521: A Binary Black Hole Merger with a Total Mass of 150 M⊙*, Physical Review Letters **125**, 10.1103/physrevlett.125.101102 (2020).

[9] Ng, Thomas C.K. Isi, Maximiliano, Wong, Kaze W.K. *et al.*, *Constraining gravitational wave amplitude birefringence with GWTC-3*, Physical Review D **108**, 10.1103/physrevd.108.084068 (2023).

[10] A. A. Trani, S. Rastello, *et al.*, *Compact object mergers in hierarchical triples from low-mass young star clusters*, Monthly Notices of the Royal Astronomical Society **511**, 1362 (2022), https://academic.oup.com/mnras/article-pdf/511/1/1362/42425280/stac122.pdf.

[11] B. P. Abbott, R. Abbott, T. D. Abbott, *et al.*, *A guide to LIGO–Virgo detector noise and extraction of transient gravitational-wave signals*, Classical and Quantum Gravity **37**, 055002 (2020).

[12] E. Thrane and C. Talbot, *An introduction to Bayesian inference in gravitational-wave astronomy: Parameter estimation, model selection, and hierarchical models*, Publications of the Astronomical Society of Australia **36**, 10.1017/pasa.2019.2 (2019).

[13] N. Jeffrey and B. D. Wandelt, *Evidence Networks: simple losses for fast, amortized, neural Bayesian model comparison*, Machine Learning: Science and Technology **5**, 015008 (2024).

[14] B. P. Abbott *et al.* (LIGO Scientific Collaboration and Virgo Collaboration), *GWTC-1: A Gravitational-Wave Transient Catalog of Compact Binary Mergers Observed by LIGO and Virgo during the First and Second Observing Runs*, Phys. Rev. X **9**, 031040 (2019).

[15] J. Veitch, V. Raymond, B. Farr, *et al.*, *Parameter estimation for compact binaries with ground-based gravitational-wave observations using the LALInference software library*, Phys. Rev. D **91**, 042003 (2015).

[16] C. M. Biwer, C. D. Capano, S. De, *et al.*, *PyCBC Inference: A Python-based Parameter Estimation Toolkit for Compact Binary Coalescence Signals*, Publications of the Astronomical Society of the Pacific **131**, 024503 (2019).

[17] G. Ashton, M. Hübner, P. D. Lasky, *et al.*, *Bilby: A User-friendly Bayesian Inference Library for Gravitational-wave Astronomy*, The Astrophysical Journal Supplement Series **241**, 27 (2019).

[18] M. Dax, S. R. Green, J. Gair, *et al.*, *Real-Time Gravitational Wave Science with Neural Posterior Estimation*, Physical Review Letters **127**, 10.1103/physrevlett.127.241103 (2021).

[19] C. Hoy and L. K. Nuttall, *BILBY in space: Bayesian inference for transient gravitational-wave signals observed*

with LISA (2023), arXiv:2312.13039 [astro-ph.IM].

[20] K. Chandra, A. Pai, S. H. W. Leong, *et al.*, *Impact of Bayesian Priors on the Inferred Masses of Quasi-Circular Intermediate-Mass Black Hole Binaries* (2023), arXiv:2309.01683 [gr-qc].

[21] J. S. Speagle, *dynesty: a dynamic nested sampling package for estimating Bayesian posteriors and evidences*, Monthly Notices of the Royal Astronomical Society **493**, 3132–3158 (2020).

[22] S. Morisaki, *Accelerating parameter estimation of gravitational waves from compact binary coalescence using adaptive frequency resolutions*, Physical Review D **104**, 10.1103/physrevd.104.044062 (2021).

[23] K. Krishna, A. Vijaykumar, A. Ganguly, C. Talbot, S. Biscoveanu, R. N. George, N. Williams, and A. Zimmerman, *Accelerated parameter estimation in Bilby with relative binning* (2023), arXiv:2312.06009 [gr-qc].

[24] S. Morisaki, R. Smith, L. Tsukada, S. Sachdev, S. Stevenson, C. Talbot, and A. Zimmerman, *Rapid localization and inference on compact binary coalescences with the Advanced LIGO-Virgo-KAGRA gravitational-wave detector network* (2023), arXiv:2307.13380 [gr-qc].

[25] D. Conor, B. Artur, M. Iain, *et al.*, *Neural Spline Flows* (2019), arXiv:1906.04032 [stat.ML].

[26] G. Papamakarios and I. Murray, *Fast ϵ-free Inference of Simulation Models with Bayesian Conditional Density Estimation* (2018), arXiv:1605.06376 [stat.ML].

[27] M. Vallisneri, *Use and abuse of the Fisher information matrix in the assessment of gravitational-wave parameter-estimation prospects*, Physical Review D **77**, 10.1103/physrevd.77.042001 (2008).

[28] U. Dupletsa, J. Harms, B. Banerjee, M. Branchesi, B. Goncharov, A. Maselli, A. Oliveira, S. Ronchini, and J. Tissino, *gwfish: A simulation software to evaluate parameter-estimation capabilities of gravitational-wave detector networks*, Astronomy and Computing **42**, 10.1016/j.ascom.2022.100671 (2023).

[29] F. Iacovelli, M. Mancarella, S. Foffa, and M. Maggiore, *GWFAST: A Fisher Information Matrix Python Code for Third-generation Gravitational-wave Detectors*, The Astrophysical Journal Supplement Series **263** (2022).

[30] J. Bradbury, R. Frostig, P. Hawkins, M. J. Johnson, C. Leary, D. Maclaurin, G. Necula, A. Paszke, J. VanderPlas, S. Wanderman-Milne, and Q. Zhang, *JAX: composable transformations of Python+NumPy programs* (2018).

[31] G. Pratten, C. García-Quirós, M. Colleoni, A. Ramos-Buades, H. Estellés, M. Mateu-Lucena, R. Jaume, M. Haney, D. Keitel, J. E. Thompson, and S. Husa, *Computationally efficient models for the dominant and subdominant harmonic modes of precessing binary black holes* (2021).

[32] R. Essick, S. Vitale, and M. Evans, *Frequency-dependent responses in third generation gravitational-wave detectors*, Phys. Rev. D **96**, 084004 (2017).

[33] S. Dwyer, D. Sigg, S. W. Ballmer, *et al.*, *Gravitational wave detector with cosmological reach*, Phys. Rev. D **91**, 082001 (2015).

[34] D. Reitze, R. Adhikari, S. Ballmer, *et al.*, *Cosmic Explorer: The U.S. Contribution to Gravitational-Wave Astronomy beyond LIGO* (2019), arXiv:1907.04833 [astro-ph.IM].

[35] J. Roulet and T. Venumadhav, *Inferring Binary Properties from Gravitational-Wave Signals*, Annual Review of Nuclear and Particle Science 10.1146/annurev-nucl-121423-100725 (2024).

[36] B. P. Abbott, A. Abel, C. Charles, *et al.* (LIGO Scientific Collaboration and Virgo Collaboration), *GWTC-3: Compact Binary Coalescences Observed by LIGO and Virgo during the Second Part of the Third Observing Run*, Physical Review X **13**, 10.1103/physrevx.13.041039 (2023).